Monitoring of water freeze – thaw cycle by means of an etched single-mode – multimode – single-mode fiber-optic refractometer

Abián B. Socorro-Leránoz, Kontxi I. Aginaga-Etxamendi, Silvia Díaz, Aitor Urrutia, Ignacio Del Villar, Ignacio R. Matias, *IEEE Fellow*

***Abstract*— As an alternative to the different technologies that permit the detection of in-situ ice formation on different surfaces, this contribution proposes the design of an etched single-mode – multimode – single-mode (E-SMS) fiber-optic-based structure as a multimode interference refractometer. This sensor provides enhanced properties with respect to a basic SMS structure, including a higher sensitivity and periodical interferometry bands that can measure surrounding refractive indices with repeatability and robustness. Since ice and water refractive indices are sufficiently different, this structure has been used to detect the freezing - thawing process of water taking place inside a freezer between -20˚C and +20˚C. Also, this work intends to show a proof of concept of a simple technology that can be applied in different situations, such as in smart cities, avionics, structural health monitoring or even to avoid a cold chain breakage. Inside, novel developments to better understand the working operation of the E-SMS structure are shown, together with a study on how to correlate optical and thermal measurements from a refractive index point of view.**

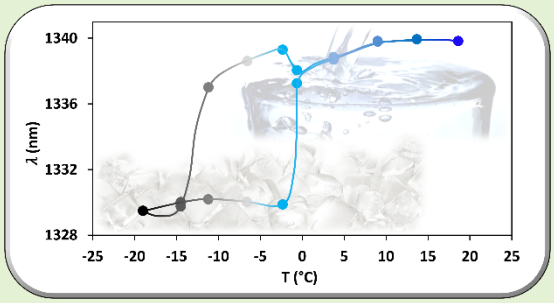

***Index Terms*— optical fiber sensors; multimode interference; ice detection; freeze – thaw cycle; refractometry**

I. Introduction

An ice detector is an instrument that detects the formation of ice on a surface. Such devices can identify the presence of icing conditions in many fields where security measures must be taken very seriously for the well-being of people working in determined sectors [1]. For instance, in aerospace engineering it is important to monitor the formation of ice in the vehicle structure during the flight, in order to avoid undesired accidents [2]. The same can be applied to the fabrication and maintenance of marine vessels, ships or submarines in naval engineering, where the fact of traveling with water around them promotes ice formation within their structures due to the cold temperatures outside [3]. Also, the monitoring of ice formation is of high importance when dealing with wind energy [4], power lines [5] or structural health monitoring (SHM) [6]. In these fields, the formation of ice leads to overload, fatigue and, in general, mechanical issues to be repaired; shutdowns affecting a whole county or breaks in the resistant materials used in bridges or roads, respectively.

Another important application in this work is the in situ prediction of ice formation in a city, which is relevant for the management of urban bus fleets, just to mention an example [7]. This parameter, along with many others, are being used in smart cities to provide information both to those who govern the cities and to the citizens themselves. The European Union, under the umbrella of the H2020 project Stardust, is developing and deploying a series of sensors initially for the lighthouse cities (Pamplona, Tampere and Trento), to later be extended to the followers and, finally, if the results are interesting, to any another European city or anywhere else [8].

Not only in the sectors previously mentioned monitoring the formation of ice is important. In the food and pharmaceutical sector there is also a need for controlling the cold chain [9]. Once the products are obtained, they must be conserved under cold temperatures, often in either refrigerated or freezing conditions, to avoid degeneration. This is the case of the freezing chambers within fishing vessels or food/drug transportation trailers, but also in the freezers and fridges existing in the supermarkets or even in home appliance, just to

Manuscript received July 21, 2022; revised April 28, 2023; accepted YYY. Date of publication ZZZ. This work was supported by the Spanish National Research Agency project with reference PID2019-106231RB-I00. Also, part of the funding was provided by the European Union's Horizon 2020 Research and Innovation Programme (Stardust-Holistic and Integrated Urban Model for Smart Cities) under Grant 774094. (Corresponding author: Abián B. Socorro-Leránoz).

Abián B. Socorro-Leránoz, Kontxi I. Aginaga-Etxamendi, Silvia Diaz, Aitor Urrutia, Ignacio Del Villar and Ignacio R. Matías are with the Department of Electrical, Electronic and Communication Engineering, Universidad Pública de Navarra (UPNA), 31006 Pamplona, Spain, and with the Institute of Smart Cities, Universidad Pública de Navarra (UPNA), 31006 Pamplona, Spain. Also, Abián B. Socorro-Leránoz, and Ignacio R. Matías are with the Navarra Institute for Health Research (IdiSNa), Recinto del Hospital Universitario de Navarra, C/ Irunlarrea 3, E-31008 Pamplona, Spain (e-mails: ab.socorro@unavarra.es, kontxiisabel.aginaga@unavarra.es, silvia.diaz@unavarra.es, aitor.urrutia@unavarra.es, ignacio.delvillar@unavarra.es, natxo@unavarra.es).

mention day-by-day applications. A break in the cold chain conditions can degenerate in bad quality products, what may lead to both money losses for companies and even health issues for the final consumers.

Tracking the evolution of a system/product under cold temperature or freezing conditions is always a challenge due to the risk of ice formation, especially when water is involved in the process. Several sensing technologies have been used for this purpose. Most ice detection systems used today are probe-style ice detectors which provide a global measurement of the icing environment, while others have been designed for specific ice detection needs. Focusing on the first group, due to their more common usage, three main strategies have been carried out. The first one is the use of electronic systems and, more specifically, capacitive sensors [10], where the water permittivity as a dielectric material varies the capacitance between two metal surfaces depending on its solid or liquid state. A second group of interest is that formed by those technologies based on microwaves [11]. Since water attenuation of microwaves is considerable, it is possible to manufacture microwave resonators whose spectral response can be modulated as a function of the liquid/solid state. Finally, the third approach is the use of thermal infrared detection [12]. Based on the emissivity of the materials, the infrared cameras can be focused to surfaces susceptible of freezing in order to measure the light attenuation induced by the formation of ice films, for example on the roads.

There is also a fourth strategy, although less explored: the use of fiber-optic sensors for the detection of icing conditions. Most of the recent contributions revised have to do with the development of distributed architectures [13], either in plastic or silica fibers [14], [15] and with different shapes to achieve a better detection of ice formation [16]. Regarding the typical fiber-optic sensors to monitor temperature, fiber Bragg gratings (FBGs), they are normally embedded inside other electrical or mechanical systems, aiming to measure strain, compensate temperature variations in case ice covers electrical transmission lines or induce pressure forces that may break the constructions, something also covered by the Stardust project [17]–[19].

The proposal suggested by this contribution relies on the fact that light propagates faster in liquid water than in ice. Based on this, there is a slight difference between the refractive indices of ice and water that can be detected with sufficient sensitivity and resolution using fiber-optic technology. In this sense, the theoretical arguments that permit this approach will be first analyzed from a physical/chemical point of view. Then, a proposal of a simple etched single-mode – multimode – single-mode (E-SMS) fiber-optic interferometer to measure the freezing – thawing cycle of water in a freezer will be addressed. A thorough characterization of the presented sensor will be shown, to prove the simplicity of the proposed method, including refractometry and repeatability measurements. Finally, several conclusions will be extracted on the use of the proposed sensor as an ice formation and freeze – thaw cycles detector.

II. Theoretical Background and Experimental Details

A. Refractive indices of Ice and Water

Using refractometry to detect ice formation relies on several contributions published between early 1970's and today. Practically all of them coincide in their estimations on what happens with the refractive indices of both solid and liquid water [20]–[27]. For the sake of simplicity, Fig. 1 depicts a summary of such estimations in the UV-NIR range, for temperatures around 20-25˚C in the case of liquid water and down to -10˚C in the case of ice [27].

Briefly, when in liquid state, the bonds between hydrogen atoms among the different molecules are loose, so water molecules can move easily without any organization. However, just at 0°C, these bonds become more stable, so water molecules start to organize in a process known as crystallization. This crystallization involves creating a hexagonal structure distributed in the space, what in the specific case of water means that there are fewer molecules in the same volume. Therefore, water molecules have to expand their volume when they freeze and thus, occupy more space. Over 4˚C, water behaves like the rest of substances: as it warms up, so does the volume. However, between 0 and 4˚C it behaves in that special way because of these specific characteristics among its hydrogen bonds. This phenomenon is known as negative thermal expansion (NTE) and, although the opposite is the behavior of most materials, there is a wide variety of materials that present NTE, such as certain kinds of silicon, complex forms of oxides and alloys [28]. It is estimated that the increase in volume experienced between 0 and 4˚C, is on the order of 10% of its volume when in liquid state. Therefore, the most important consequence is that when water freezes, it loses density [29].

On the other hand, within the VIS-NIR range, where this work is focused on, the refractive index of water does not vary so much in comparison to the rest of the spectrum. In particular, the absorption coefficient is practically null and that is why it is not analyzed any more. Almost the same applies to the real part. However, it can be observed that ice and water are slightly

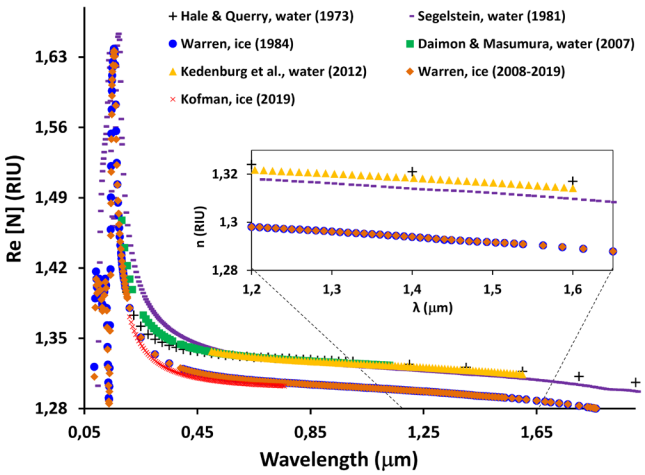

Fig. 1. Spectral evolution of the refractive indices of liquid water and ice. Only the real part is plotted, in view that the absorption coefficient in this spectral range is practically null and does not present significant variations. Data extracted from [18]–[25].

different, with an average value of near 1.318 RIU in the case of liquid water and near 1.295 RIU in the case of ice. Although the difference is quite small, the fact of being less dense is what makes the ice present less resistance to the light propagation, and that is why its refractive index is lower. Additionally, these values present a slight decrease within the second and third communications window (see Fig. 1 inset), although both curves remain parallel. Consequently, if an optical phenomenon is sensitive and resolutive enough, it will be possible to discern between water and ice refractive indices in this spectral range.

B. Considerations to design the E-SMS structure

The interest in publishing sensing solutions using the single-mode – multimode – single-mode (SMS) fiber-optic structure has been reclaimed recently. A review by Wu et *al.* [30] has tried to collect all the strategies that have emerged around this structure since the beginning, supporting their affirmations with a convincible mathematical background. The main conclusion is that it is always possible to obtain a multimode interferometer by just breaking the propagation symmetry along the optical waveguide. Depending on this and the selection of the fiber segments used to induce the interferometry, different patterns of spectral shapes can be obtained, with selectable values of sensitivity and resolution.

In this sense, in this work it has been decided to keep on exploring the features of the SMS structure, consisting of a segment of no core or coreless fiber spliced between a couple SMF-28 pigtails, in order to obtain a simple interferometer with enhanced evanescent field (see Fig. 2a). This optical waveguide has been deeply studied in several contributions with the goal of obtaining a simple, easy-to-fabricate, easy-to-handle and cost-effective structure for research. It has been used for a wide variety of applications, including refractometry [31], measurement of liquid level [32] or even biosensing [33]. An optimization of the structure has been also analyzed, in order to obtain adequate responses for various sensing applications [34].

The underlying operating principle of light propagation in an SMS structure is the multimode interference excited due to the modes beating inside the coreless segment, which can be influenced by external perturbation. This interference can be seen as a coupling of light from the input SMF to several modes in the coreless segment [34]. Light propagates through different modes inside the coreless segment, and hence the phase of the modes is different when all of them interfere at the coreless - output SMF interface.

The transmission attains a maximum if the length of the coreless segment is selected so that the field distribution at the multimode – monomode interface is an image of the input field [35]. This phenomenon is commonly known as self-imaging effect (SI or SI band) and its central wavelength can be tuned by an adequate selection of the parameters in the well-known expression (1) [34]–[36]:

$$\lambda = \frac{4pD^2}{L} \cdot n \;\; ; \;\; p = 1,2,3,\ldots \qquad (1)$$

where D and n are the waveguide diameter and its refractive index, respectively, and λ is the operational wavelength. The integer factor p denotes the periodic nature of the SI effect along the waveguide.

Regarding the SMS structure sensitivity to surrounding refractive index (SRI), there is an agreement with the fact that its improvement does not rely on the length of the coreless segment [34]. Briefly, the length of the coreless segment only contributes to modify the obtained spectrum due to the different propagation constants of the interfering modes. Depositing a high-refractive index thin-film onto the optical structure has been also studied. In this case, part of the light transmitted through the coreless segment is coupled inside the thin-film and, if deposited in optimal conditions, it is possible to increase the sensitivity of the SMS structure [34], [37]. A third strategy is splicing a reduced diameter coreless segment to the single-mode (SMF) pigtails [38], naming the structure as etched-SMS (E-SMS). By combining both coating and etching, it is possible to reach high variations that enhance the behavior of these multimode interferometers [39]. In this sense, when facing the ice formation detection pursued in this work, with an optimized SMS structure it will be possible, not only to detect the ice formation, but also to track the freeze – thaw cycle with a clear distinction in every phase of the process by just taking a look to the refractive index changes in the external medium.

Thus, a strategy based on etching an SMS structure was used for the sake of simplicity. To this purpose, a simulation based on the finite difference method FDM of FIMMWAVE® (Photon Design Inc.) was first performed, with the goal of studying the behavior of the optical waveguide. According to

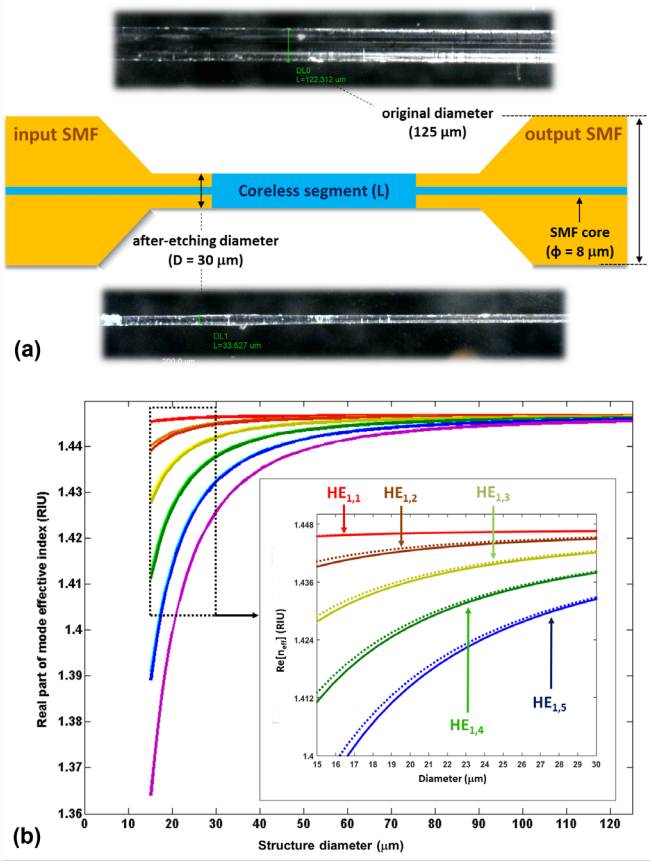

Fig. 2. (a) Schematic of the E-SMS structure used with insets of the etching process. (b) Real part of the mode effective index evolution for the 10 first modes propagating in the E-SMS structure as a function of the decreasing diameter. The inset shows HE modes in air (SRI = 1.000 RIU solid lines) and water (SRI = 1.321 RIU – dashed lines).

[40], in an optical fiber with circularly symmetric index perturbation in any transverse plane of the structure, only coupling between modes with azimuthal order 1 occurs. This is the case of the analyzed structure. Hence, hybrid modes $HE_{1,1}$, $HE_{1,2}$, $HE_{1,3}$, etc., and $EH_{1,1}$, $EH_{1,2}$, $EH_{1,3}$, etc. were considered. Regarding the SMF section, only the fundamental mode $HE_{1,1}$ was simulated because light is basically transmitted through the core. In the case of the coreless segment, 30 modes were simulated, a number that was considered sufficient to achieve a convergence in the results.

Taking into account these considerations, Fig. 2b shows an increasing separation among the effective indices of the modes guided within the coreless section as a function of the decreasing diameter. This is due to the lower number of modes guided in this section as its diameter is reduced. Here it is important to point out that the simulated modes are hybrid modes, either HE or EH, due to the cylindrical symmetry of the optical structure. It can be observed that as the SMS diameter decreases, so does the effective index of each mode, following a logarithmic shape according to FDM. Each one of the curves corresponds to a mode originally propagating within the coreless segment, which decreases its effective index as the structure diameter is reduced. Additionally, the inset shows the difference between the modes analyzed in air and water, respectively. Only HE modes are plotted for simplicity. The zoom allows to see that all modes present a higher contrast from air to water for a lower diameter in the E-SMS structure. This occurs because the diameter reduction leads to a higher interaction of the lower order modes analyzed in Fig. 2a with the surrounding medium, which improves the sensitivity [41].

C. Setting up the optical configuration.

The optical set-up used for the experiments is described in this section. Every E-SMS sensor was manufactured by splicing a 14 mm-length coreless fiber segment (POFC Inc.) to two standard SMF-28 pigtails from Telnet Redes Inteligentes S.A. One of the SMF pigtails was connected to a white SLED light source (HP-83437A) and the other one to an HP-86142A optical spectrum analyzer (OSA). Here, it is important to remark that the whole structure should remain straight in order to avoid non-desired interferences due to bending or a wrong etching process. To this purpose, the E-SMS structure was glued to a glass framework.

Once the original substrate was fabricated, the etching process was performed. According to Fig. 2b, as the diameter of the waveguide is reduced, more modes are cutoff. This involves a higher interaction with the SRI and also a higher sensitivity. However, it was decided to etch the structure from a diameter of 125 microns to 30 microns, with the goal of avoiding non-desired mechanical effects when freezing as well as significant signal loss. This was possible by immersing the substrate in 40% hydrofluoric acid (HF - Sigma Aldrich Inc.) for 50 minutes, as indicated in [42]. This process was monitored online, using an IEEE 488 bus communication through MATLAB® in order to obtain the desired spectrum that will be analyzed in section 3. Some measurements related to sensitivity to SRI were also performed, including an experiment of stability and repeatability.

Then, to achieve the ice formation detection, Figs. 3a and 3b show the double optical-electronic monitoring prepared in order to correlate both data. First, the same optical transmission set-up described previously with the E-SMS was used to obtain the spectral behavior. Secondly, a standard electronic circuit based on an operational amplifier and an INA118 connected to an Arduino Uno board was designed to map the voltage values from a T-type thermocouple to temperature. A T-type thermocouple was used due to its convenient characteristics when providing stable and real-time temperature measurements under freezing conditions [43]. Both the E-SMS and the thermocouple were introduced in a freezer through a wall bushing made on one of its sides. Inside the freezer, they were fixed in a plastic bowl, immersed in a 3-5 mm-thickness film of water and then subjected to freezing - thawing cycles to monitor both the electrical and the optical evolution at the same time.

III. Results and Discussion

A. Monitoring the etching process

As mentioned in section 2c, an E-SMS structure with 14 mm-length coreless segment and a diameter of 30 microns was used. A simple way to control this process and tune the spectrum where desired is by representing the obtained transmission spectrum of the E-SMS as its diameter is being reduced. Thus, a first spectrum is obtained without the original SMS structure and the subsequent spectra are all referred to this initial one,

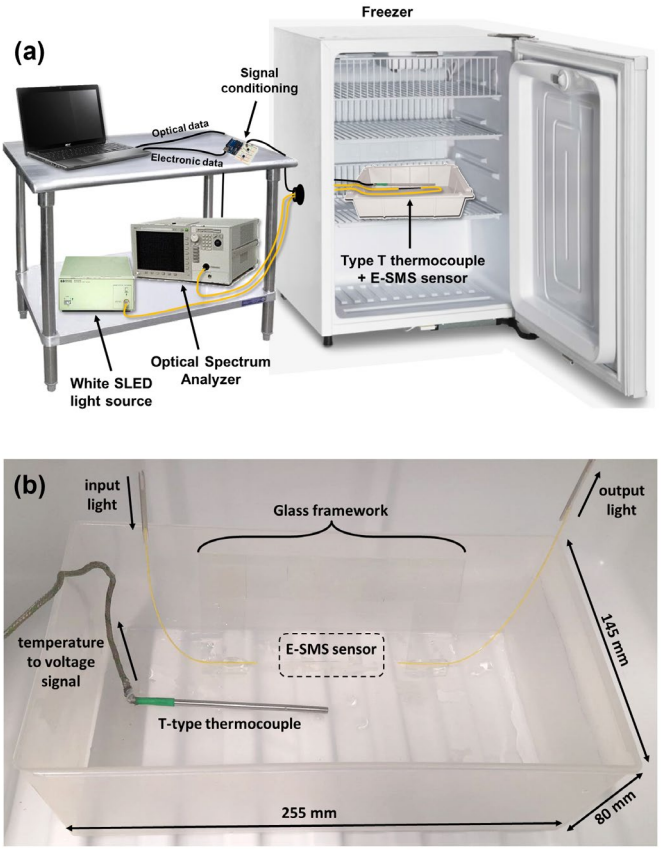

Fig. 3. (a) Experimental set-up used to detect ice formation. (b) Plastic bowl with both electrical and optical sensors inside the freezer. Cables collect the corresponding signals in the different domains for simultaneous optical and electrical monitoring of the process. Just 5 mm of water height are poured to obtain a crystal ice film covering both sensors.

obtaining the transmission spectrum of the E-SMS structure as the etching takes place. A visualization of this etching process can be found as supplementary file in [42], showing the spectral evolution both numerically (using FIMMWAVE®) and experimentally. In order to complement this visualization, the transmission values obtained with the OSA are mapped as a function of both the wavelength and the decreasing diameter in Figs. 4a and 4b for the specific E-SMS structure used in this study. Here, the Sellmeier equation in [44] was used as cladding refractive index. Additionally, due to the fact of dealing with a standard SMF-28 fiber, a 0.36% was added to get the core index. SMF original core and cladding diameters were adjusted to 8 and 125 microns. The final diameter of the etched area was decremented to 30 microns in 2 μm steps. The SRI value outside the fiber was adjusted to 1.22 to simulate that the fiber was immersed in HF. Many attenuation and transmission bands show up along the process, as a product of the interference among the modes involved inside the coreless segment. Both experimental and numerical results coincide quite well, so the estimated behavior is corroborated when reducing the structure diameter to 30 μm.

At this point, two aspects deserve to be analyzed. The first one is related to the shift of the interferometric bands. As the etching process takes place, there is a blue-shift of the whole spectrum. By analyzing expression (1), it may be straightforward inferred that in order to find an SI band in the spectrum for a fixed coreless segment length, it is necessary to search for lower wavelengths as the diameter decreases. The same occurs to the rest of the spectrum. This is very useful when manufacturing this type of structures, since it is possible to obtain a better reproducibility by stopping the etching process at a desired point.

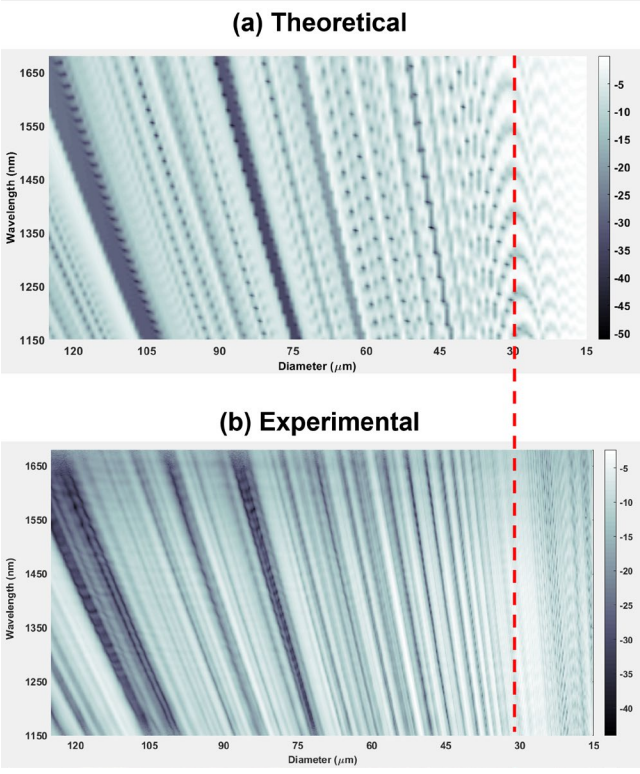

Fig. 4. (a) Numerical and (b) experimental results obtained when subjecting an E-SMS structure to HF-etching. The spectrum blue-shifts as a function of the decreasing diameter, giving the possibility of tuning the interferometry bands where desired. The red-dashed line indicates the point where the etching of the E-SMS used in this contribution has been stopped. For more information on how the etching process is reflected in the E-SMS spectrum, it is convenient to visualize the timelapses provided by reference [39] as supplementary material.

B. Refractometry measurements

A typical experiment to characterize the sensitivity of optical fiber sensors is to immerse them in different solutions with varying refractive indices and register the overall wavelength shift of the spectral bands obtained. Thus, several solutions containing increasing percentages of glycerin in water were prepared, obtaining refractive indices from 1.321 to 1.408 RIU.

The results comparing the sensitivity of the SI band using a 125 micron-diameter SMS and an interferometric band using the 30 micron-diameter E-SMS, both within the third communications window are analyzed in Fig. 5a. As it can be observed, numerical and experimental results fit quite well along the refractive index range analyzed. In the case of the 125 micron-diameter SMS, the sensitivity is 183 nm/RIU, whereas the sensitivity for the 30 micron-diameter E-SMS is 776 nm/RIU. This supposes an increasing factor of 4.24, meaning that the latter sensor shows increased sensitivity to SRI.

A more accurate analysis can be done between 1.295 and 1.318 RIU, the refractive index range of interest for this application (grey-shadowed in Fig. 5a). Taking the values provided by the theoretical estimation, a wavelength shift of 3.148 nm is attained. According to this, the sensitivity is 136.87 nm/RIU for the E-SMS, whereas in the case of the non-etched structure, the wavelength shift hardly reaches 1 nm, so the estimated sensitivity is 43.478 nm/RIU. Therefore, the E-SMS structure presents a 3.148-fold sensitivity improvement with respect to the simple SMS structure. This value is slightly reduced with respect to the 4.24-fold previously calculated, but the wavelength shift obtained between 1.295 and 1.318 RIU is also lower than 1.321 to 1.408 RIU, so this slight reduction in the sensitivity factor makes sense. Moreover, Figs. 5b and 5c represent the spectral evolution of the obtained E-SMS interferometric band located at 1200 nm in water as a function

of the varying SRI for two cycles. Results suggest good repeatability with this increased sensitivity. Again, the reason for this behavior is an increase of the interaction between the lower order modes guided in the coreless section and the external medium [40], what can be translated as an increase in the effective index variation as a function of SRI.

C. Monitoring of water freeze / thaw cycles

Once the sensitivity to SRI was analyzed, the next step was to monitor the water liquid-to-solid state change and vice versa. To this purpose, a dual electrical – optical monitoring is represented in Figs. 6a to 6d as evidence of the synchronized behavior that all the spectral bands of the E-SMS structure show as the different stages of the process take place. Together with the electrical monitoring of the temperature using the T-type thermocouple, each one of the subplots correspond to the time response for three interferometric bands originally located at 1238, 1340 and 1611 nm respectively.

During this experiment, two freeze-thaw cycles were monitored, each one corresponding to a whole day. In every cycle, first the freezer cooled down the temperature from +20˚C to -20˚C, a process that usually takes around 3.5 hours. Then, it was disconnected from the electrical network, and the thawing process took place spontaneously during the next 20 hours, moment when it was reconnected.

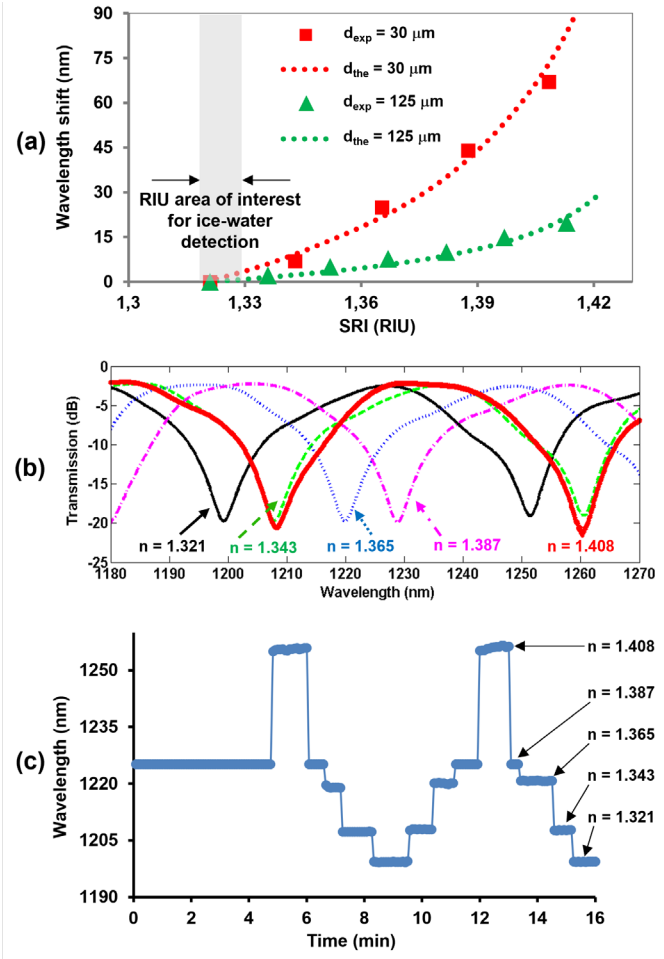

Fig. 5. (a) Numerical and experimental wavelength shifts for SMS structures with diameters of 125 and 30 μm respectively. The tracking of the interfering bands of interest is plotted for different SRIs in the third communications window. (b) Wavelength shift experienced by an interference band at 1200 nm, which repeatability is represented in (c). The different refractive index values correspond to solutions of 0, 10, 35, 50 and 65% v/v of glycerin in ultrapure water. RI values taken with a Mettler Toledo® commercial refractometer at room temperature with an accuracy of ±0.0003 RIU.

An analysis of the different stages is performed in the following lines, similar to what Wahl et *al.* do in [45]. As it can be observed in Fig. 6 and Fig. 7, four main stages are distinguished. Additionally, for the sake of simplicity and due to the closeness of the interfering band located at 1340 nm to the second optical communications window, a specific analysis of Fig. 6b is carried out in Fig. 7 for a single freeze / thaw cycle.

First, the interferometric bands blue-shift progressively during the cooling process until reaching 0˚C by means of temperature sensitivity, which is a convolution of the thermo-optic properties of both the E-SMS structure and the water [45], [46]. After half an hour, water starts to freeze by losing its latent heat of fusion. Fifty minutes later, all the water has turned into ice. Here, the grey dashed line in Fig. 6 indicates the moment where the optical response starts to decrease dramatically until a sudden decrease is registered (see grey arrows highlighting these points). Specifically, a 3 nm shift in the case of p3 can be observed in Fig. 7 inset. The reason for this behavior is that it gets to a point where all the water has frozen and the SRI outside the fiber is 1.295, according to [22]. Therefore, the sensitivity of the E-SMS to SRI is higher than its sensitivity to temperature and that is why this fast decrease occurs. During

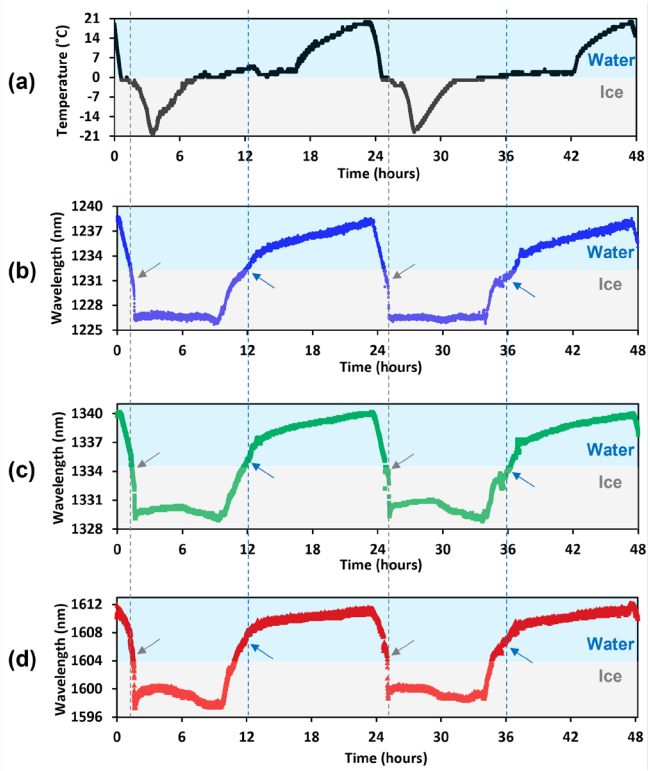

Fig. 6. 2 cycles of 1-day time showing the matching between the electrical response (a) and optical response of interfering bands p1 (b), p3 (c) and p5 (d). Grey arrows indicate the moment when all the water is frozen. Blue arrows indicate the moment when all the ice has melted, becoming liquid water.

This article has been accepted for publication in IEEE Sensors Journal. This is the author's version which has not been fully edited and
content may change prior to final publication. Citation information: DOI 10.1109/JSEN.2023.3273226

these first 1.5 - 2 hours of decreasing temperature stage, the total wavelength shift of these interferometric bands is on the order of 12-15 nm, depending on the analyzed peak.

During the second stage, either freezing or heating, both Fig. 6 and Fig. 7 show that the optical response remains quite constant, although the interferometric bands may experience a slight shift. For instance, a maximum of 2 nm are registered for the 1611 nm band (p5), whereas 1.5 nm can be noticed in the case of p3 and p1 seems not to shift. Additionally, all wavelength shifts occur in an opposite way than in the case of temperature shift and they are not the same from cycle to cycle. Once the ice film surrounds the optical structure, these slight oscillations are attributed to strain interactions between the ice film and the optical waveguide [45]. In spite of being under ice refractive index conditions, this strain can be detected due to the interferometric nature of the E-SMS, which makes it sensitive to deformations, both when the ice induces them and also when they cease because the temperature is sufficiently close to 0ºC and therefore, the ice starts to melt. That is why the interferometric band returns to the final freezing wavelength. In this sense, both strain and refractive index effects overlap to obtain the visualized response.

Continuing with the dynamic response, the third stage occurs between hours 9 and 13 (or either 34 and 38 in the second cycle), when ice melts slowly, again, acquiring the latent heat of fusion. Because this process is carried out spontaneously inside the freezer chamber, the thermocouple response remains increasing with a very slow rate around 0ºC, meaning that the ice film is turning into water. In the case of the E-SMS, the response is clearly noticeable. In these conditions, the ice refractive index increases to that of the liquid water by means of a new thermo-optic variation both in the ice and in the sensor that is transduced as a red-shift in wavelength [45], [46].

Moreover, around one hour before finishing this third stage, some curves in Fig. 6 and Fig. 7 experience variations in their rate of change. This can be also corroborated in SD where, indeed, depending on the interferometric band considered, the response is variable. According to [45], this is attributed to a combined presence of remaining ice pieces and water on the E-SMS surface, what influences its response. Additionally, and making use of Fig. 2b analyzed previously, the presence of both ice and water along the sensitive area of the E-SMS induces a variable effective refractive index, which can locally either increase or decrease the number of modes effectively propagating through the structure. This may induce slight shifts of the interferometric bands to either longer or shorter wavelengths.

Finishing with the fourth stage, up from hour 13 to 24 (38 to 48 in the second cycle), the presence of liquid water is higher than that of the ice and this will remain as such until all the ice is melted. This is why the thermocouple, which was oscillating close to 0ºC, ends up recovering temperature once the recipient only contains water. From the E-SMS point of view, once the sensor surrounding medium is water, its response is symmetric to what happened in the first stage. Therefore, the red-shift visualized is again due to a convolution of the thermo-optic properties of the E-SMS structure and the water until reaching both the original temperature (+20˚C) and the original wavelength location.

After this study, the combined analysis of both thermocouple and E-SMS sensor permits to distinguish two clear areas in the optical response, depending on whether the E-SMS sensor is

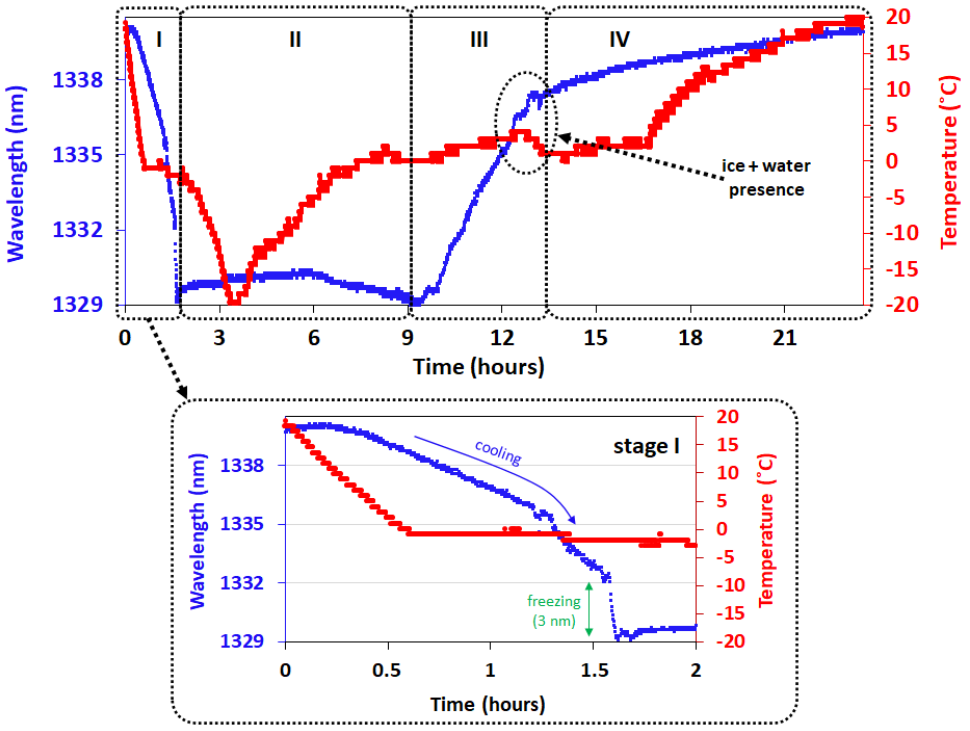

Fig. 7. The 4 different stages described in section III.C for the specific case of the interferometric band p3. The inset shows the cooling and freezing stages for both temperature and E-SMS sensors. As in Fig. 6, the electrical resolution (Arduino board) is 1ºC, whereas the optical resolution (OSA) is 0.1 nm for a 430 nm span between 1250 and 1680 nm. The OSA accuracy is ±0.2 nm.

surrounded by water or ice. In this sense, if the temperature remains below 0ºC, once the sensor is inside the ice, the response is quite constant and no considerable effects except ice strain shall vary the location of the interferometric bands, with a negligible contribution of the temperature variation. On the other hand, if the sensor is surrounded by water, the thermo-optic coefficients of both water and E-SMS are combined, leading to a progressive variation, more similar to the temperature variation, either while cooling (induced by the freezer) or while heating up (spontaneously). The fact of working with an increased sensitivity interferometer facilitates the clear distinction of the different phenomena analyzed, which are a combination between sensitivities to SRI and the thermo-optic coefficients of the materials involved. The same behavior can be observed for both freezing – thawing cycles during the 2-day experiment, what gives an idea of the process repeatability. Attached to this contribution, the supporting document SD shows more evidence regarding how the interfering bands of the E-SMS structure monitor the freeze – thaw process.

To finish this contribution, a complementary point of view is addressed in Fig. 8. Again, this analysis will be focused on the p3 band, although the SD document contains the information related to all the interferometric bands analyzed in this article.

Fig. 8a shows the spectral shape of the p3 band and its wavelength location at different moments of the cooling / freezing process. Then, by tracking the wavelength shift of p3 along time during a complete freeze/thaw cycle, Fig. 8b can be plotted. Three main areas are worth commenting by taking a look to Fig. 8b. The first one, between +20ºC and 0ºC, where the sensitivity attained is ±100 pm/˚C in average, with a maximum slope of ±182 pm/˚C (between +13ºC and 0ºC), both for water cooling down and heating up. When freezing, a maximum slope of -1500 pm/ºC is obtained when the E-SMS is about to be surrounded by ice completely. Unlike in the case of the liquid state, this remarkable slope change near one order of magnitude is attributed to the fact that losing/gaining the latent heat of fusion induces a sudden wavelength shift in comparison to what happens in the liquid state. Then, while frozen, the freezer keeps decreasing the temperature to -20ºC. However, this temperature variations do not actually induce a remarkable sensitivity. All the water is frozen so, despite some slight variations previously associated to the strain suffered by the optical structure within the ice film [45], it could be said that the spectral behavior is stable, and no shifts should be considered. This also indicates that the SRI in the proximities of the E-SMS sensor remains quite constant, something that the sensor captures properly. Regarding the thawing process, it occurs at a practically constant temperature due to the endothermic nature of the reaction, so it does not make sense to establish a sensitivity.

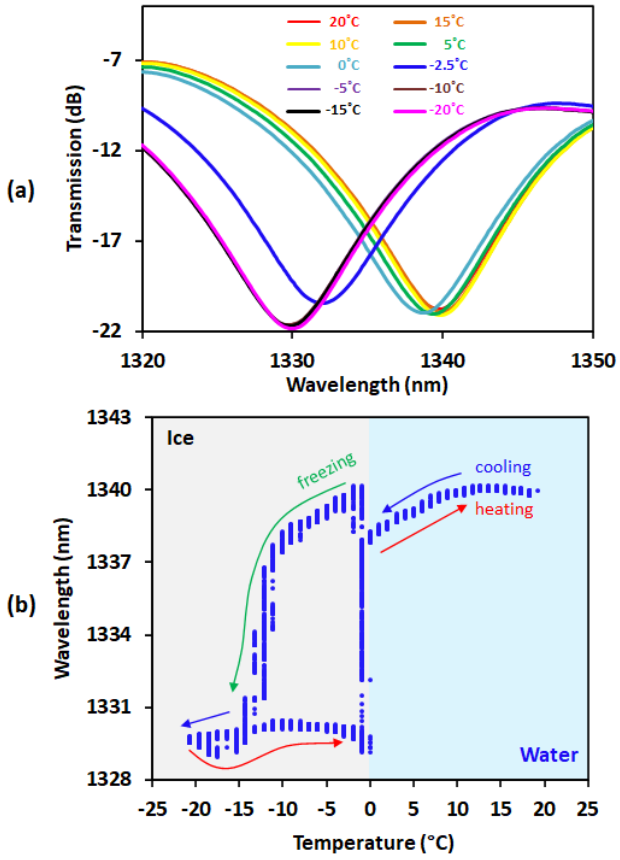

Fig. 8. (a) Spectral behavior of p3 interferometric band during the freezing process, from +20˚C to -20˚C. (b) Optical vs temperature characterization curve of the freezing - thawing process based on the wavelength location of p3 band at every stage. The information for every interferometric band in this work can be found in SD document.

Apart from that, it is worth speaking about hysteresis. As it can be observed, the freezing process forced by the freezer compressor needs to go down below -5˚C or even -10ºC inside the chamber to produce the water solidification. Water freezes progressively from the surface to the inside. Only when the water molecules surrounding the fiber freeze is when this sudden change can be observed. The same happens when thawing, but in this case between 0ºC and 2ºC. Since water starts melting from the surface to the inside, those molecules surrounding the fiber remain frozen until they all become liquid. Is then when a sudden refractive index change is observed, apparently, while water heats up to higher temperatures. Therefore, the sensor clearly detects the presence of either ice or water, but also the freezing - thawing processes.

IV. Conclusion

Under the European Stardust project, this work shows some results related to the detection not only of ice formation based on a multimode interference optical fiber sensor, but also a simple strategy to monitor the freezing – thawing process of a liquid such as water. This is a very important parameter to consider for urban traffic in a city and for many other applications such as trains, constructions, etc. However, during the completion of this work, more highlights have been achieved, which are discussed below.

First, more light has been shed on how and etched single-mode – multimode – single-mode (E-SMS) structure works. Specifically, a numerical simulation has been presented to explain the way it is possible to enhance the sensitivity of this structure to surrounding refractive index as a function of the decreasing diameter. Thanks to this, a 4.24-fold sensitivity

increase has been attained by just reducing the diameter to 30 μm. This is due to reducing the effective refractive indices of the modes involved within the optical waveguide as the diameter decreases. Even more sensitivity is expected to obtain with a thinner diameter, although this may lead to mechanical issues when handling it that may prevent its use in the smart city application for which this sensor has been developed.

Second, the sensitivity enhancement has been combined to an adjustment of the coreless segment with the goal of obtaining a spectrum with several resolutive interference bands. This has added more robustness when detecting wavelength shifts as a function of the surrounding refractive index, while permitting more reproducibility and stability in the measurements.

The previous enhancements have been used to detect both progressive and sudden changes in the refractive index of the sensor surrounding medium. In this contribution, an optical fiber E-SMS-based interferometer has been used as a refractometer to monitor the processes occurring when cooling down water temperature, which varies between average values of 1.295 and 1.318 RIU when in solid and liquid states, respectively. This freezing – thawing cycle comprises 4 main stages. When the water temperature is either cooling down or heating up in liquid state, a slight variation in the wavelength shift of the interferometric bands can be registered by means of temperature sensitivity. Once the water is frozen, there are no significant wavelength shifts, since the ice film is already formed. However, is in the transition between solid-to-liquid and vice versa states where significant changes are observed as noticeable wavelength shifts. These changes can be attributed to the way water freezes or melts starting from the surface and finishing inside. Also, the influence of the thermo-optic effect of both water and the optical structure and the strain, modify the attained response, which can be transduced in terms of optical variations. This, together with the fact of detecting the phase change with increased sensitivity, allows the E-SMS structure to monitor the freezing – thawing process of water.

In the opinion of the authors, this opens the way for future research on the use of simple multimode interferometers such as the one presented in this work not only in smart city applications, such as structural health monitoring of buildings and civil constructions, urban fleet management, trains and airports, etc, but also in many others such as, for example, in the detection of breaks in the cold chain in the agri-food sector.

REFERENCES

[1] D. G. Jackson and J. I. Goldberg, “Ice detection systems: A historical perspective,” *SAE Tech. Pap.*, no. 724, pp. 776–790, 2007.

[2] R. ; Hann and T. A. Johansen, “Unsettled Topics in Unmanned Aerial Vehicle Icing,” 2020.

[3] J. E. . Overland, C. H. . Pease, and R. W. Preisendorfer, “Prediction of Vessel Icing,” *J. Clim. Appl. Meteorol.*, vol. 25, no. 12, p. 13, 1986.

[4] M. C. Homola, P. J. Nicklasson, and P. A. Sundsbø, “Ice sensors for wind turbines,” *Cold Reg. Sci. Technol.*, vol. 46, no. 2, pp. 125–131, 2006.

[5] M. Farzaneh, *Atmospheric Icing of Power Networks*. Chicoutimi (Canada): Springer, 2008.

[6] J. Andre, A. Kiremidjian, Y. Liao, C. Georgakis, and R. Rajagopal, “Structural health monitoring approach for detecting ice accretion on bridge cable using the Haar Wavelet Transform,” in *Proc. SPIE 9803, Sensors and Smart Structures Technologies for Civil, Mechanical, and Aerospace Systems 2016*, 2016.

[7] STARDUST project, https://stardustproject.eu/ (accessed May 02, 2023).

[8] J. J. Astrain, F. Falcone, A. J. Lopez-Martin, P. Sanchis, J. Villadangos, and I. R. Matias, “Monitoring of Electric Buses within an Urban Smart City Environment,” *IEEE Sens. J.*, vol. 22, no. 12, pp. 11364–11372, 2021.

[9] R. Badia-Melis, U. Mc Carthy, L. Ruiz-Garcia, J. Garcia-Hierro, and J. I. Robla Villalba, “New trends in cold chain monitoring applications-A review,” *Food Control*, vol. 86, p. 13, 2018.

[10] A. Troiano, E. Pasero, and L. Mesin, “New system for detecting road ice formation,” *IEEE Trans. Instrum. Meas.*, vol. 60, no. 3, pp. 1091–1101, 2011.

[11] B. Wiltshire, K. Mirshahidi, K. Golovin, and M. H. Zarifi, “Robust and sensitive frost and ice detection via planar microwave resonator sensor,” *Sensors Actuators, B Chem.*, vol. 301, no. August, pp. 2–6, 2019.

[12] M. Riehm, T. Gustavsson, J. Bogren, and P. E. Jansson, “Ice formation detection on road surfaces using infrared thermometry,” *Cold Reg. Sci. Technol.*, vol. 83–84, pp. 71–76, 2012.

[13] A. A. Ikiades, “Direct ice detection based on fiber optic sensor architecture,” *Appl. Phys. Lett.*, vol. 91, no. 10, pp. 1–4, 2007.

[14] K. Amiropoulos, D. Spasopoulos, and A. Ikiades, “Fiber optic sensor for ice detection on aerodynamic surfaces using plastic optic fiber tapers,” *Opt. InfoBase Conf. Pap.*, vol. Part F110-, pp. 5–6, 2018.

[15] J. Zou, L. Ye, J. Ge, and C. Zhao, “Novel fiber optic sensor for ice type detection,” *Meas. J. Int. Meas. Confed.*, vol. 46, no. 2, pp. 881–886, 2013.

[16] K. Amoiropoulos, G. Kioselaki, N. Kourkoumelis, and A. Ikiades, “Shaping beam profiles using plastic optical fiber tapers with application to ice sensors,” *Sensors (Switzerland)*, vol. 20, no. 9, 2020.

[17] Z. Liu, Z. Zhang, C. Liu, and L. Li, “Application of strain difference model and FBG sensor to power transmission line ice monitoring,” *Asia Commun. Photonics Conf. ACPC 2015*, vol. 0, pp. 2–4, 2015.

[18] L. Zhao and X. Huang, “Integrated condition monitoring system of transmission lines based on fiber bragg grating sensor,” *C. 2016 - Int. Conf. Cond. Monit. Diagnosis*, no. 1, pp. 667–670, 2016.

[19] J. Wei, Y. Hao, Y. Fu, L. Yang, J. Gan, and Z. Yang, “Detection of glaze icing load and temperature of composite insulators using fiber bragg grating,” *Sensors (Switzerland)*, vol. 19, no. 6, 2019.

[20] G. M. Hale and M. R. Querry, “Optical Constants of Water in the 200-nm to 200-μm Wavelength Region,” *Appl. Opt.*, vol. 12, no. 3, p. 555, 1973.

[21] D. J. Segeistein, “The Complex Refractive Index of water,” 1981.

[22] S. G. Warren, “Optical constants of ice from the ultraviolet to the microwave,” *Appl. Opt.*, vol. 23, no. 8, p. 20, 1984.

[23] M. Daimon and A. Masumura, “Measurement of the refractive index of distilled water from the near-infrared region to the ultraviolet region,” *Appl. Opt.*, vol. 46, no. 18, pp. 3811–3820, 2007.

[24] S. G. Warren and R. E. Brandt, “Optical constants of ice from the ultraviolet to the microwave: A revised compilation,” *J. Geophys. Res. Atmos.*, vol. 113, no. 14, pp. 1–10, 2008.

[25] S. Kedenburg, M. Vieweg, T. Gissibl, and H. Giessen, “Linear refractive index and absorption measurements of nonlinear optical liquids in the visible and near-infrared spectral region,” *Opt. Mater. Express*, vol. 2, no. 11, p. 1588, 2012.

[26] V. Kofman, J. He, I. Loes ten Kate, and H. Linnartz, “The Refractive Index of Amorphous and Crystalline Water Ice in the UV–vis,” *Astrophys. J.*, vol. 875, no. 2, p. 131, 2019.

[27] S. G. Warren, “Optical properties of ice and snow,” *Philos. Trans. R. Soc. A Math. Phys. Eng. Sci.*, vol. 377, no. 2146, 2019.

[28] P. J. Attfield, “Mechanisms and materials for NTE,” *Front. Chem.*, vol. 6, no. AUG, pp. 1–6, 2018.

[29] M. Arthur, D. Saffer, and P. Belmont, “Water: Science and Society. Thermal expansion and density,” *InTeGrate (Interdisciplinary Teaching about Earth for a Sustainable Future). Open Courseware by both The Pennsylvania State University and the Utah State University*, 2022. [Online]. Available: https://www.e-education.psu.edu/earth111/. [Accessed: 08-Mar-2022].

[30] Q. Wu *et al.*, “Singlemode-Multimode-Singlemode Fiber Structures for Sensing Applications-A Review,” *IEEE Sens. J.*, vol. 21, no. 11, pp. 12734–12751, 2021.

[31] I. Del Villar, A. B. Socorro, J. M. Corres, F. J. Arregui, and I. R. Matias, “Refractometric sensors based on multimode interference in

a thin-film coated single-mode-multimode-single-mode structure with reflection configuration.," *Appl. Opt.*, vol. 53, no. 18, pp. 3913–3919, 2014.

[32] O. Fuentes *et al.*, "Increasing the Sensitivity of an Optic Level Sensor With a Wavelength and Phase Sensitive Single-Mode Multimode Single-Mode Fiber Structure," *IEEE Sens. J.*, vol. 17, no. 17, p. 5515, 2017.

[33] A. B. Socorro *et al.*, "Fiber-Optic Immunosensor Based on an Etched SMS Structure," *IEEE J. Sel. Top. QUANTUM Electron.*, vol. 23, no. 2, 2017.

[34] I. Del Villar *et al.*, "Optimization of Sensors Based on Multimode Interference in Single-Mode – Multimode – Single-Mode Structure," *J. Light. Technol.*, vol. 31, no. 22, pp. 3460–3468, 2013.

[35] A. Mehta, W. Mohammed, and E. G. Johnson, "Multimode interference-based fiber-optic displacement sensor," *IEEE Photonics Technol. Lett.*, vol. 15, no. 8, pp. 1129–1131, 2003.

[36] N. S. Fabian, A. B. Socorro-Leranoz, I. Del Villar, S. Diaz, and I. R. Matias, "Multimode-Coreless-Multimode Fiber-Based Sensors: Theoretical and Experimental Study," *J. Light. Technol.*, vol. 37, no. 15, pp. 3844–3850, Aug. 2019.

[37] A. B. Socorro, I. Del Villar, J. M. Corres, F. J. Arregui, and I. R. Matias, "Sensitivity enhancement in a multimode interference-based SMS fibre structure coated with a thin-film: Theoretical and experimental study," *Sensors Actuators, B Chem.*, vol. 190, pp. 363–369, 2014.

[38] Q. Wu, Y. Semenova, P. Wang, and G. Farrell, "High sensitivity SMS fiber structure based refractometer--analysis and experiment.," *Opt. Express*, vol. 19, no. 9, pp. 7937–44, Apr. 2011.

[39] Y. Cardona-Maya, A. B. Socorro, I. Del Villar, J. L. Cruz, J. M. Corres, and J. F. Botero-Cadavid, "Label-free wavelength and phase detection based SMS fiber immunosensors optimized with cladding etching," *Sensors Actuators, B Chem.*, vol. 265, 2018.

[40] T. Erdogan, "Cladding-mode resonances in short- and long- period fiber grating filters," *J. Opt. Soc. Am. A. Opt. Image Sci. Vis.*, vol. 14, no. 8, pp. 1760–1773, 1997.

[41] S. Silva *et al.*, "Ultrahigh-sensitivity temperature fiber sensor based on multimode interference," *Appl. Opt.*, vol. 51, no. 16, p. 3236, 2012.

[42] Y. Cardona-Maya, I. Del Villar, A. B. Socorro, J. M. Corres, I. R. Matias, and J. F. Botero-Cadavid, "Wavelength and Phase Detection Based SMS Fiber Sensors Optimized with Etching and Nanodeposition," *J. Light. Technol.*, vol. 35, no. 17, 2017.

[43] M. Duff and J. Towey, "Two Ways to Measure Temperature Using Thermocouples Feature Simplicity, Accuracy, and Flexibility," *Analog Dialogue*, vol. 44, no. 10, pp. 1–6, 2010.

[44] I. H. Malitson, "Interspecimen Comparison of the Refractive Index of Fused Silica*,†," *J. Opt. Soc. Am.*, vol. 55, no. 10, p. 1205, 1965.

[45] M. S. Wahl, Ø. Wilhelmsen, and D. R. Hjelme, "Using fiber-optic sensors to give insight into liquid-solid phase transitions in pure fluids and mixtures," *Exp. Therm. Fluid Sci.*, vol. 119, no. October 2019, p. 110198, 2020.

[46] S. Novais, M. S. Ferreira, J. L. Pinto, "Determination of thermo-optic coefficient of ethanol-water mixtures with optical fiber tip sensor," *Optical Fiber Technology*, vol. 45, pp. 276-279, 2018.